UCRL-JC-118610
PREPRINT

Numerical Simulation of a Wave-Guide Mixing Layer on a CRAY C-90

J.A. Greenough
W.Y. Crutchfield
C.A. Rendleman

This paper was prepared for submittal to the
26th American Institute of Aeronautics and Astronautics
Fluid Dynamics Conference
San Diego, CA
June 19-22, 1995

April 1995

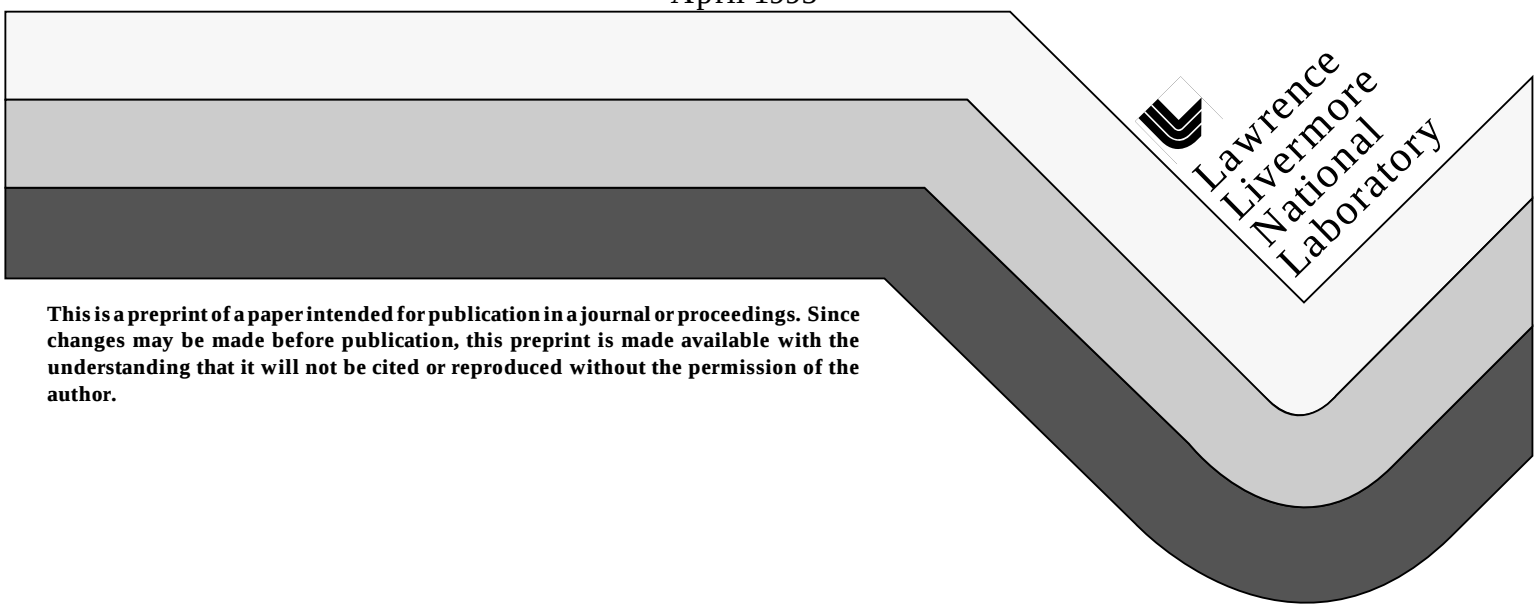

NUMERICAL SIMULATION OF A WAVE-GUIDE MIXING LAYER ON A CRAY C-90 *

Jeffrey A. Greenough, William Y. Crutchfield & Charles A. Rendleman

Center for Computational Sciences and Engineering
Lawrence Livermore National Laboratory
Livermore, CA 94550

May 19, 1995

Abstract

The development of a three-dimensional spatially evolving compressible mixing layer is investigated numerically using a parallel implementation of Adaptive Mesh Refinement (AMR) on a Cray C-90. The parallel implementation allowed the flow to be highly resolved while significantly reducing the wall-clock runtime. A sustained computation rate of 5.3 Gigaflops including I/O was obtained for a typical production run on a 16 processor machine. A novel mixing layer configuration is investigated where a pressure mismatch is maintained between the two inlet streams. In addition, the sonic character of the two streams is sufficiently different so that the pressure relief wave is trapped in the high speed stream. The trapped wave forces the mixing layer to form a characteristic cellular pattern. The cellular structure introduces curvature into the mixing layer that excites centrifugal instabilities characterized by large-scale counter-rotating vortical pairs embedded within the mixing layer. These are the dominant feature of the flow. Visualizations of these structures in cross-section show the pumping action which lifts dense fluid up into light gas. This effect has a strong impact on mixing enhancement as monitored by a conserved scalar formulation. Once the large-scale structures are well established in the flow and undergo intensification from favorable velocity gradients, the time-averaged integrated product shows almost a four-fold increase. A spectral analysis of the flowfield over the cellular structures, as part of a full space-time analysis, shows these structures to be zero-frequency modes that develop from low level essentially broad-banded noise. This characterization of the vortical structures and their appearance is consistent with a recent linear stability analysis of a mixing layer over a curved wall that predicts the most unstable modes to be zero frequency streamwise vortices. Time series spectral analysis of the spanwise velocity in the far field, near outflow, shows an inertial range in the mid to high frequencies. Above this region is a clear dissipative range out to the Nyquist frequency with no anomalous accumulation of energy at or near the highest frequencies.

*This work of these authors was performed under the auspices of the U.S. Department of Energy by the Lawrence Livermore National Laboratory under contract No. W-7405-Eng-48. Support under contract No. W-7405-Eng-48 was provided by the Applied Mathematical Sciences Program of the Office of Energy Research. Partial support was provided by the HPCC Grand Challenge Project in Computational Fluid Dynamics and Combustion Dynamics. Computations were carried out on the National Energy Research Supercomputing Center's Cray C-90 under the Special Parallel Processing Allocation.

Introduction

A mixing layer can be thought of as a simple model for the injection process that occurs in combustors and propulsion systems. In such system, the co-flowing streams of fuel and oxidizer are mixed by large scale motions and entrain-

ment and also by the actions of molecular diffusion. In high speed flows, the large scale motions are known to be significantly modified by the increased Mach number. Among the effects are the inhibition of large-scale vortical structure formation, decreased entrainment and mixing of the fluids, and a decrease in the overall layer growth [1], [2], [3], [4].

Attempts to overcome the decreased instability of high speed shear flows has lead to the investigation of alternative scenarios for mixing enhancement. This line of investigation has included studies aimed at understanding the effect of walls [5], [6] and shock interactions on the development of mixing layers [7]. The presence of walls has been shown to result in new families of instability modes. But direct simulations have shown that these wall modes do not play an important role in the transition process [8]. Using a shock wave to enhance mixing provided marginal enhancement [7]. But that may be more a result of the artificial way the shock wave was introduced into the domain than the effect of a shock wave on the mixing layer.

The present numerical study addresses the development of a three-dimensional spatially evolving mixing layer in a high speed regime that exhibits a different development than has been previously investigated. This flow has a convective Mach number near unity with one stream subsonic and one stream supersonic. The flow is confined within a rectangular duct thus introducing wall effects. Also, a shock wave is introduced naturally into the flow by maintaining a pressure mismatch between the in-flowing streams, a common occurrence in practical systems.

The pressure mismatch results in a shock wave emanating from the splitter plate and propagating into the lower high speed stream. In addition, the deflection of the shear layer leads to baroclinic production of spanwise vorticity across the layer. The sonic difference between the two streams is sufficiently large so that the wave is trapped entirely within the the dense high speed layer. The ducting of the wave and the expansion/compression pattern resulting from interaction with the free surface results in a characteristic cellular structure. A schematic of this configuration is shown in figure 1. We refer to the x direction as the streamwise direction, y is the vertical direction and z is the spanwise direction.

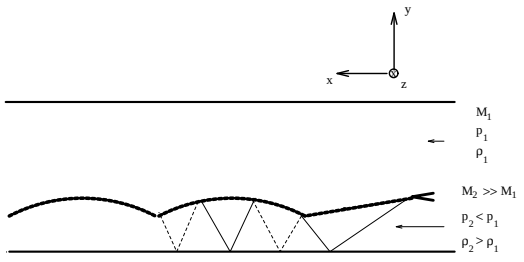

Figure 1: Schematic showing cellular structure formed by the shock wave and mixing layer interaction. The arrows show the relative inflow velocities. The solid lines represent the shock/compression waves, the small dashed lines represent expansion wave trains and the heavy dashed line represents the location of the mixing layer.

The interactions of the oblique shock wave with the mixing layer introduces perturbations to the velocity and density fields of the mixing layer. Hence the trapped compression wave serves two purposes:(1) to introduce curvature onto the mixing layer and (2) to introduce finite three-dimensionality into the mixing layer.

The curvature of the mixing layer leads to embedded, or for simplicity referred to later as streamwise vortices, vortices formated in a manner similar to that for Görtler vortices in the the boundary layer or Taylor vortices in Couette flow. That is, there is vortex stretching (enhancement) exerted by favorable velocity gradients in the curved mixing layer plane. This leads to intensification of the vortical perturbations thus forming counter-rotating vortex tubes embedded within the mixing layer plane. There is an important difference between the present case and other centrifugal instabilities (e.g., the Görtler case). In this one the high speed flow is inside, relative to the curvature, and next to the wall.

In the Görtler case, there is low speed flow next to the wall. A recent linear stability analysis for mixing layers over curved walls for the case where the high speed flow is inside, relative to the curvature predicts the most unstable modes to be zero phase streamwise vortices [9]; precisely the type of structures observed.

Contrary to other high speed mixing layer configurations, the present one produces a flow field dominated initially by large-scale streamwise vortical structures. These structures take the place of spanwise rollers found in low speed flow and provide an efficient means for pumping fluid between the two streams due to their long streamwise extent. The computation is carried out through a flow field transition characterized by a breakdown from the large-scale coherent streamwise vortices to that of complicated finescale vortical structures.

The development of a parallel version of AMR has allowed studying the flow development at a high level of resolution while reducing the elapsed wall-clock time compared to simulating the flow on a single processor. Also, using the machine in dedicated mode allowed using essentially the entire solid state disk (SSD) as a large I/O buffer (approximately 200 megawords) before writing to disk. With this approach, we were then able to use the SSD as a large buffer for writing asynchronously to rotating disk without incurring a CPU penalty. Intelligent design of I/O dataflow was required to accommodate the large amount of data generated for the space-time analysis and for generating flowfield visualizations.

Problem Description

The inlet conditions are that of a non-pressure matched subsonic/supersonic mixing layer with an asymmetric placement of the splitter plate (see figure 1). The gases are assumed to have equal γ's set to 1.4. We nondimensionalize the variables in the problem by choosing the lower channel width times 1.5 as the reference length, the upper stream density as the reference density and the upper inlet pressure (divided by γ) as the reference pressure. Note that these choices gives the upper stream inlet sound speed as one. This reduces the parameter space of the problem to three parameters. Namely, they are inlet velocity ratio, inlet pressure ratio, and inlet density ratio. The asymmetry in width between the upper and lower channel inlets is about 4 to 1.

The initial conditions are $U_{upper}/U_{lower} = 3$, $p_{upper}/p_{lower} = 3.6$ and $\rho_{upper}/\rho_{lower} = .25$. These conditions give an upper stream inlet Mach number of 0.3 and a lower stream inlet Mach number of 3.4.

Overall, the domain size is 65 (x) by 4 (z) by 6.5 (y), where x is the streamwise direction, y is vertical and z is spanwise. The effective resolution on the finest grid (see next section) is 1040(x) by 104(y) by 64(z) cells.

The flow is perturbed in all three velocity components over two momentum thicknesses about the splitter plate by 2% of the mean streamwise velocity times a random amplitude between zero and one.

Methodology

The equations used to model this flow are the Euler equations for an ideal gas. They are solved in conservative form using the higher-order Godunov method developed by Colella [10]. This is a high resolution finite difference algorithm that robustly treats flow discontinuities, has a local nonlinear dissipation mechanism for suppression of spurious oscillations, provides accurate treatment of nonlinear wave structure by solving a local Riemann problem and has low phase error properties. The nonlinear dissipation mechanism provides a means for dissipating kinetic energy in a smooth fashion into internal energy thus acting as a high wavenumber sink. This mechanism occurs automatically without incorporation of an explicit sub-grid dissipation model.

A conserved scalar formulation is used as a diagnostic tool to assess mixing. It provides a simple model for an infinite rate, irreversible, no heat release, binary reaction. This reduces to solving an additional advection equation for the density weighted scalar. From the scalar, the individual species can be computed.

The higher-order Godunov integrator is utilized by an Adaptive Mesh Refinement (AMR) shell based on the original ideas of Berger and

Oliger [11] and later by Berger and Colella [12]. The AMR methodology enables simulation of complex problems by reducing the computational and storage requirements by concentrating the computational effort in regions requiring high accuracy. The computational effort is concentrated by locally refining the computational grid and generating a hierarchy of grids. It has been successfully used for a wide variety of problems in both two-dimensions [12] and three-dimensions [13]. In the current implementation, all grids are considered logically rectangular. AMR provides the means for managing the grid hierarchy. This includes regridding, advancing (in time) grids, and synchronizing (in time) the grid hierarchy. The AMR shell is implemented in C++ while the higher-order Godunov integrator is implemented in FORTRAN [15].

The current problem had one level of refinement over the base grid. The refinement ratio between the base grid and the refined level was four. Near the inlet, the refinement was restricted below a vertical level of two length units. After transition, the refinement was restricted below a vertical level of four length units. Overall, 40% of the domain was refined to the highest level.

The overhead associated with the the manipulation of the AMR data structures in the C++ part of the code is small. Most of the time is spent executing floating point operations on regular rectangular arrays which are very efficiently compiled in FORTRAN. As a result, the program as a whole reaches speeds of over 390 megaflops on a single C-90 processor.

A parallel shared-memory version of AMR was developed as part of the National Energy Research Supercomputing Center's (NERSC) Special Parallel Processing Allocation (SPPA). The parallel implementation was used for this application and run on the NERSC C-90 using 16 processors. See [14] for details of the implementation. The implementation utilizes a coarse-grained approach to parallelism in which each grid is integrated forward in time by a single processor. With approximately 100 grids on the finest level of refinement, there is abundant opportunity for parallelism. High parallel efficiency is achieved using a ready-queue approach [14].

Due to the large amount of data required for space-time analysis and visualization, optimizations were needed to to avoid disk I/O slow-down. The Solid State Disk (SSD) had a large buffer allocated on it to which the CPU wrote data. Once the data is written there, the CPU is free to continue computation. The I/O Cluster bypasses the CPU and writes the data in the buffer asynchronously to rotating disk. The I/O speedup when compared to directly writing to disk was approximately 30.

A representative timing of a production run using this methodology on the 16 processor NERSC C-90 achieves an average rate of 5.293 gigaflops as measured using the hardware performance monitor. This included start-up and shut-down I/O and writing 8.1 gigabytes of data in 307 files over the course of the run. Wall clock time was 9300 seconds and used 128,209 CPU seconds.

Flow field Analysis

The computational domain contains approximately 4.2 millions zones so saving all of the data at every time step is not feasible. Specialized data structures, referred to as slabs, were constructed so that a coarsened representation of the data was saved at each coarse grid time step (after all transients had passed and the statistics where stationary). These structures preserve the refined spatial representation of the data where it exists. Data was saved at 65 locations downstream over the full cross section of the domain. This gives a streamwise spatial resolution of approximately 10 slabs per cellular structure, or one slab every streamwise length unit.

We also have the entire flowfield available for a fixed point in time. In figure 2 slices in the x-y plane of the density field (see coordinate system in figure 1 for orientation) are shown for four z coordinate locations. Note that cellular structure and the pressure relief wave. Downstream of the second cell, the flow character changes from highly organized to three-dimensional structure exhibiting intermittancy and large fluctuations.

The effect of the streamwise structures is primarily to pump dense fluid upward forming mushroom structures. In figure 3 four density field planes are over the backside of the second

cell. The first frame is at the apex of the curvature, continuing through transition. The denser fluid is colored dark gray and it penetrates into the lighter gas. The lighter gas penetrates much less into the heavy gas due the reduced density.

From the conserved scalar formulation, the formation of product can be used as a crude measure of mixing. The time averaged values of the computed product are integrated over each of the data acquisition slabs (integrated in y and z coordinate directions) and are shown as a function of streamwise coordinate in figure 4. For reference, the first cell has extent in nondimensional length units, $5 < x < 16$, and the second cell, $16 < x < 25$. Over the first cell, there is minimal mixing; probably limited by numerical diffusion. But over the second cell, where the streamwise structures are fully formed and undergoing strong intensification, there is almost a four-fold increase in integrated product. After the transition, there is another factor of two increase in product, but the rate of production is substantially decreased and is decreasing with downstream distance.

The downstream evolution of the streamwise vortices is analyzed by examining the spanwise sine transform of the fluctuating vertical velocity for the first few lowest frequencies. Recall that $\partial v/\partial z$ is a component of the streamwise vorticity. The first plot, figure 5, shows the spanwise power spectra at the apex of the first cell for the four lowest discrete frequencies. The vertical location for the analysis is in the mid-plane of the mixing layer. The zero frequency component is at a very weak power level for all modes and $\omega = 0.08$ frequency component is the most dominant. As we move downstream to the apex of the second cell (shown in figure 6), at the mixing layer mid-plane vertically, we see that the zero frequency $\omega = 0.0$ component is the dominant one. Note that the spectra for the higher frequencies not shown are at a significantly lower power level from those displayed. This is in agreement with the theoretical prediction of Liou that a curved layer of this type has most unstable modes that are zero-frequency streamwise vortices. Furthermore, our visualizations show that these structures are indeed streamwise vortices that occur in counter-rotating pairs. This is an important result since it shows that the mixing layer curvature necessary to generate streamwise vortices can arise in a more general setting where the curvature is due to trapped wave interactions rather than a curved bounding wall.

Time series spectra analysis of the spanwise velocity in the far field, five length units before the outflow boundary, is shown in figure 7. It shows an inertial range at the mid to high frequencies. Above this region is a clear dissipative range out to the Nyquist frequency. There is no anomalous accumulation of energy at or near the highest frequencies.

References

[1] Chinzei, N., Masaya, G., Komuro, T., Murakami, A., Kudou, K., 1986, Spreading of two-stream supersonic mixing layer, Phys. Fluids A*29* (5), pp. 1345-1347.

[2] Papamoschou, D., Roshko, A., 1986, Observations of supersonic free shear layers, AIAA paper 86-0126.

[3] Papamoschou, D., Roshko, A., 1988, The compressible turbulent shear layer: an experimental study, J. Fluid Mech., *197*, pp. 453-477.

[4] Papamoschou, D., 1989, Structure of the compressible turbulent shear layer, AIAA paper 89-0126.

[5] Tam, C.K.W., Hu, F.Q., 1989, The instability and acoustic wave modes of supersonic mixing layers inside a rectangular channel, J. Fluid Mech. *203*, pp. 51-76.

[6] Greenough, J.A., Riley, J.J., Soetrisno, M., Eberhardt, D.S., 1989, The effects of walls on a compressible mixing layer, AIAA paper 89-0372.

[7] Lu, P.J., Wu, K.C., 1991, On the shock enhancement of confined supersonic mixing flows, Phys. Fluids A *3* (12), pp. 3046-3062.

[8] Gathmann, R.J., Si-Ameur, M., Mathey, F., Numerical simulations of three-dimensional natural transition in the compressible confined shear layer, Phys. Fluids A*5* (11), pp. 2946-2968.

[9] Liou, W.W., 1994, Linear instability of curved free shear layers, Phys. Fluids *6* (2), pp. 541-549.

[10] Colella, P. 1985, A direct eulerian MUSCL scheme for gas dynamics, SIAM J. Sci. Stat. Comput., pp. 104-117.

[11] Berger, M.J., Oliger, 1984, Adaptive mesh refinement for hyperbolic partial differential equations, J. Comp. Phys. *53*, pp. 484-512.

[12] Berger, M.J., Colella, P., 1989, Local adaptive mesh refinement for shock hydrodynamics, J. Comp. Phys., *82*, pp. 64-84.

[13] Bell, J.B., Berger, M.J., Saltzman, J., Welcome, M., three dimensional adaptive mesh refinement for hyperbolic conservation laws, UCRL-JC-108794, to appear in SIAM J. Sci. Stat. Computing.

[14] Crutchfield, W.Y. 1994, A parallel adaptive mesh refinement algorithm on the C-90, ERSUG paper.

[15] Crutchfield, W.Y. and Welcome, M.L., 1993, Object-oriented implementation of adaptive mesh refinement algorithms, Scientific Programming, vol. 2, pp. 145-156.

[16] Greenough, J.A., Bell, J.B., Direct simulation of a shock-induced mixing layer, 1993, UCRL-JC-112208.

[17] Greenough, J.A., Bell, J.B., Direct numerical simulation of a shock-induced mixing layer, 1993, J. Fluid Mech., in review.

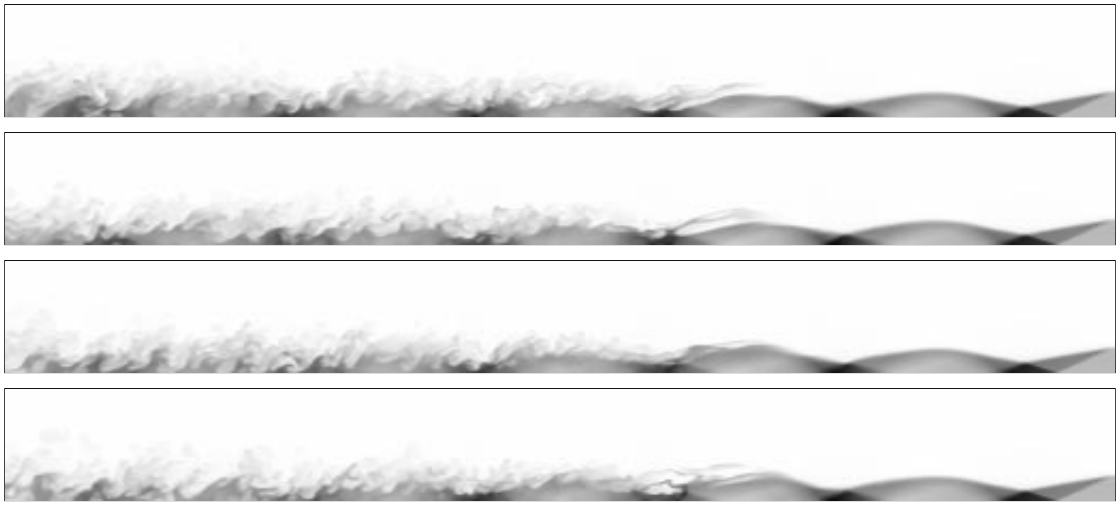

Figure 2: The density field is shown for four spanwise locations. The inlet is at the right. The pressure relief wave emanating from the splitter plate is visible in the dense high speed layer. Note the two cellular structures. Downstream of the second cell the flow transitions to a highly three-dimensional state.

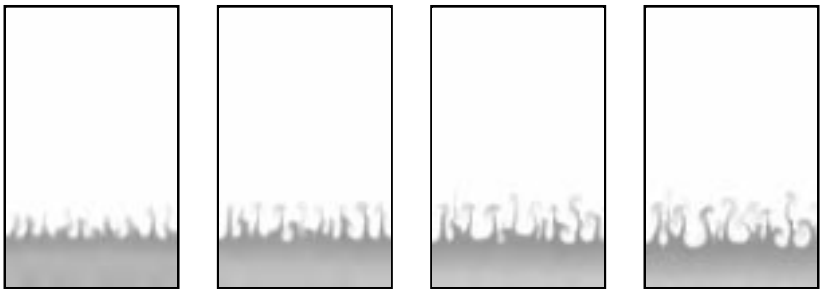

Figure 3: The density field is shown for four streamwise locations. The slices begin at the apex of the second cell and end at the end of the cell, near the transition region. The pumping action of the streamwise vortices is evident by the mushrooms formed in the mixing layer. The denser gas (dark gray) penetrates deeply into the light gas forming long fingers with mushroom caps.

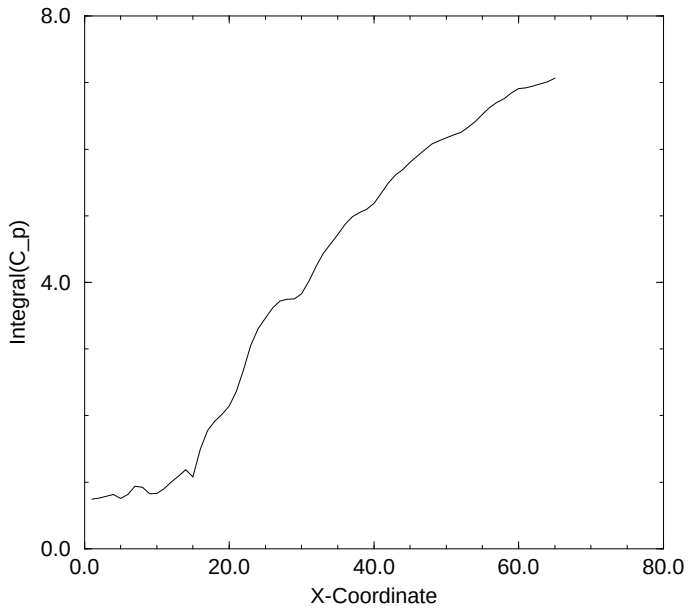

Figure 4: The time averaged product, integrated over the spanwise cross-section, is shown as a function of streamwise coordinate. For reference, the first cell has extent, $5 < x < 16$, and the second cell has extent, $16 < x < 25$. There is minimal mixing over the first cell, while there is an almost four-fold increase in the amount of integrated product over the second cell. After transition, the rate of increase decreases but with another two-fold amount of integrated product.

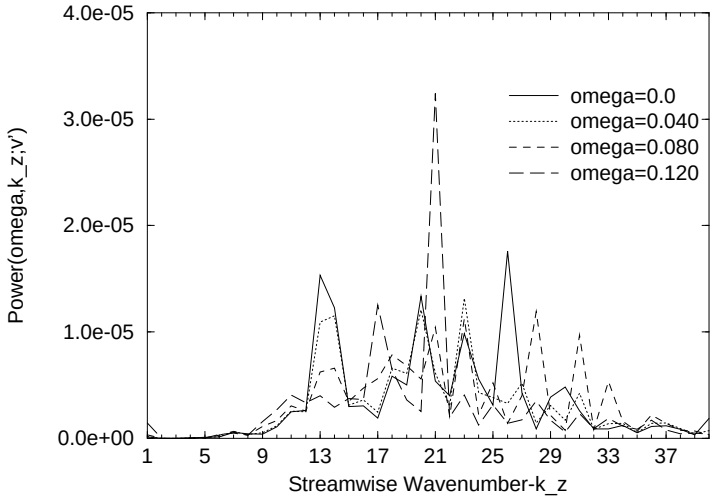

Figure 5: The spanwise power spectrum of the fluctuating vertical veloctity is shown for four discrete frequencies for a vertical location at the mid-line of the mixing layer and a streamwise location at the first cell apex. The zero frequency ($\omega = 0.0$) component is at a very power level.

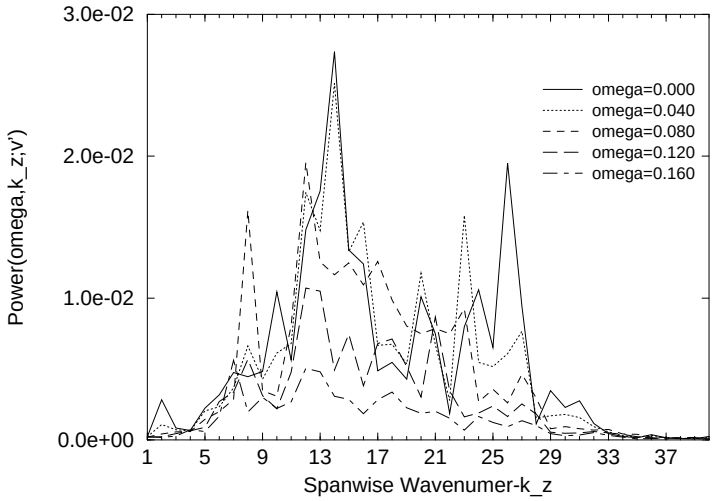

Figure 6: The spanwise power spectrum of the fluctuating vertical veloctity is shown for five discrete frequencies for a vertical location at the mid-line of the mixing layer and a streamwise location at the second cell apex. The zero frequency ($\omega = 0.0$) component is the dominant frequency.

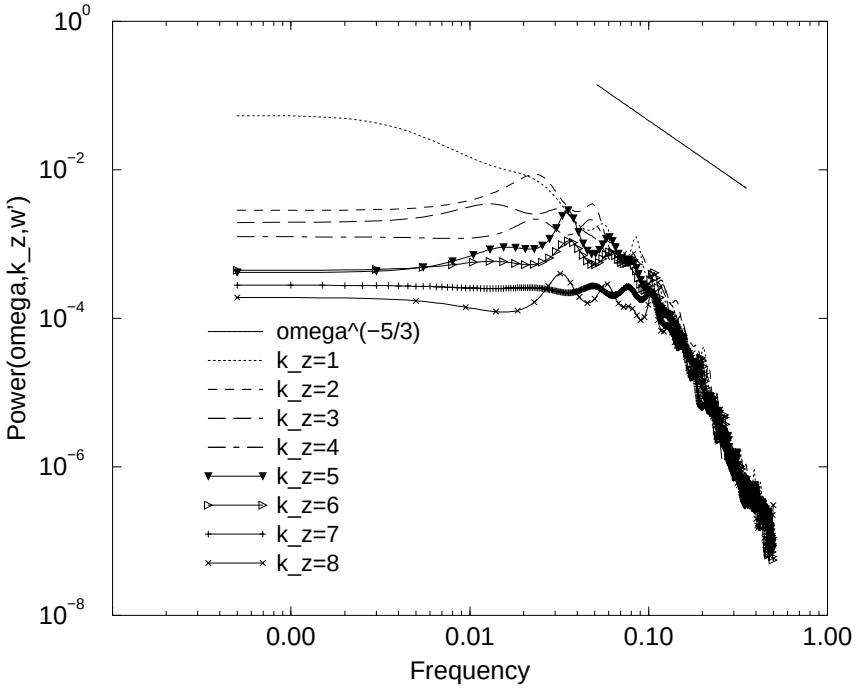

Figure 7: The far field time series spectral analysis of the spanwise velocity, five length units before the outflow boundary, is shown for the 8 lowest wavenumbers. It shows an inertial range at the mid frequencies. Above this region is a clear dissipative range out to the Nyquist frequency. There is no anomalous accumulation of energy at or near the highest frequencies.

Technical Information Department • **Lawrence Livermore National Laboratory**
University of California • Livermore, California 94551